

# Robust Features for Snapshot Hyperspectral Terrain-Classification

Christian Winkens<sup>(✉)</sup>, Volkmar Kobelt, and Dietrich Paulus

Active Vision Group, Institute for Computational Visualistics,  
University of Koblenz-Landau, Koblenz, Germany  
{cwinkens, vkobelt, paulus}@uni-koblenz.de

**Abstract.** Hyperspectral imaging increases the amount of information incorporated per pixel in comparison to normal RGB color cameras. Conventional spectral cameras as used in satellite imaging use spatial or spectral scanning during acquisition which is only suitable for static scenes. In dynamic scenarios, such as in autonomous driving applications, the acquisition of the entire hyperspectral cube at the same time is mandatory. We investigate the eligibility of novel snapshot hyperspectral cameras which capture an entire hyperspectral cube without requiring moving parts or line-scanning. Captured hyperspectral data is used for multi class terrain classification utilizing machine learning techniques. Prior to classification, the data is segmented using Superpixel segmentation which is modified to work successfully on hyperspectral data. We further investigate a simple approach to normalize the hyperspectral data in terms of illumination, which yields vast improvements in classification accuracy, preventing most errors caused by shading and other influences. Furthermore we utilize Gabor texture features which add spatial information to the feature space without increasing the data dimensionality in an excessive fashion. The multi-class classification is evaluated against a novel hyperspectral ground truth dataset specifically created for this purpose.

**Keywords:** Hyperspectral imaging · Terrain classification · Spectral analysis · Autonomous vehicles

## 1 Introduction and Motivation

Spectral imaging is defined by acquiring light intensity for pixels in an image. Each pixel stores a vector of intensity values, which corresponds to the incoming light over a defined wavelength range. Typically, researchers utilize sensors like these on Landsat, SPOT satellites or the Airborne Visible Infrared Imaging Spectrometer (AVIRIS) systems. These line scanning sensors provide information of the Earth's surface and allow static analysis. This area has been firmly established for many years and is essential for several applications like earth observation, inspection and agriculture. Additionally onboard realtime hyperspectral image analysis for autonomous navigation is an exciting and promising application scenario. But this topic is relatively unexplored because the established hardware is only capable of capturing static scenes. This is due to the scanning requirements for constructing a full 3-D hypercube of a scene. Using line-scan

cameras, multiple lines need to be scanned, while with cameras using special filters, several frames have to be captured to construct an spectral image of the scene. The slow acquisition time is responsible for motion artifacts which impede the observation of dynamic scenes. Therefore, new sensor techniques and procedures are needed here. This drawback can be overcome with novel highly compact, low-cost, snapshot mosaic (SSM) imaging cameras, which are able to capture a whole spectral cube in one shot. The capture time is considerably shorter than that of filter wheel solutions allowing to capture a hyperspectral cube at one discrete point in time. Utilizing these sensors, it is possible to use hyperspectral camera systems on unmanned land vehicles and utilize them for continuous terrain classification while moving. Most classifiers for spectral classification treat hyperspectral data as a set of spectral measurements and do not consider spatial dependencies. So the data is classified only based on their spectral information. These approaches discard information associated with correlations among neighboring pixels. Joint spectral and spatial classification techniques seem reasonable to address these disadvantages.

In this paper we investigate the use of snapshot mosaic hyperspectral cameras on unmanned land vehicles for drivability analysis and evaluate different spectral and contextual features for hyperspectral classification based on the data we captured. We make use of established supervised classifiers to recognize different classes like drivable, rough and obstacle which can be seen as terrain recognition or environmental perception based on spectral reflectances.

The remainder of this paper is organized as follows. In the following section an overview of common algorithms for feature extraction and spectral classification is given. Then our general setup is presented in Sect. 3. Our feature extraction and classification approach is described in detail in Sects. 4 and 5. And in Sect. 6 we present our results on our new hand-labeled dataset. Finally a conclusion of our work is given in Sect. 7.

## 2 Related Work

The standard procedure for image-based terrain classification is defined by capturing regular RGB images and trying to identify different classes, like Chetan et al. [9] did. They used color information and local binary patterns (LBP) in combination with different supervised classifiers. Additionally, in recent years, hyperspectral classification has been under active development. Hyperspectral data allows for a more detailed insight into the composition and nature of materials like plants and soil than standard RGB data. Although there are some unsupervised classification algorithms in literature, we focus on supervised classification for the moment, because it is more widely used as shown by Plaza et al. [21]. Most supervised classifiers suffer from the Hughes effect [14], especially when dealing with high-dimensional hyperspectral data. To deal with this issue, Melgani et al. [18] and Camps-Valls et al. [5] introduced support vector machines with adequate kernels for hyperspectral classifications. Supervised techniques are limited by the availability of labeled training data and suffer from the high dimensionality of the data. While recording data is usually quite straightforward, the precise and correct annotation of the data is very time-consuming and complicated. Therefore semi-supervised

techniques have come up to fix this as proposed by Camps-Valls et al. [7]. Jun et al. [16] presented a semi-supervised classifier that selects non-annotated data based on its entropy and adds it to the training set. The classification of hyperspectral data reveals several important challenges. There is a great mismatch between the high dimensionality of the data in the spectral range, its strong correlation and the availability of annotated data, which is absolutely necessary for the training. Another challenge is the correct combination and integration of spatial and spectral information to take advantage of features from both these domains.

In various experiments by Li et al. [17] it was observed that classification results can be improved by investigating spatial information in parallel with the spectral data. Different efforts have been made to incorporate context-sensitive information in classifiers for hyperspectral data [21]. Fauvel et al. [10] fuse morphological and hyperspectral data to enhance classification results. As a consequence, it has now been widely accepted that the combined use of spatial and spectral information offers significant advantages. To integrate the context into kernel-based classifiers, a pixel can be simultaneously defined both in the spectral domain and in the spatial domain by applying a corresponding feature extraction. Contextual features are achieved, for example, by the standard deviation per spectral band. This leads to a family of new kernel methods for hyperspectral data classification reported by Camps-Valls et al. [6] and implemented using a support vector machine. Brown et al. [4] used principal component analysis for dimensionality reduction and proposed an extension of the well known SIFT descriptor, called multi-spectral SIFT (MSIFT) for scene category recognition. Salamati et al. [22] investigated different combinations of SIFT and spectral information to enhance recognition accuracy. An alternative approach to combining contextual and spectral information is the use of Markov random fields (MRFs). They exploit the probabilistic correlation of adjacent labels [23].

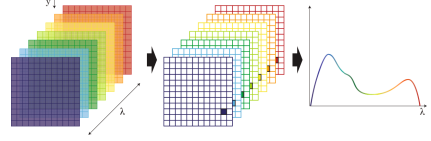
In comparison there is only little research in literature on hyperspectral classification utilizing terrestrial spectral imaging, where data was not captured from an earth orbit or an airplane but from cameras which were mounted on land-based vehicles. One example is the vegetation detection in hyperspectral images as demonstrated by Bradley et al. [2], who showed that the use of the Normalized Difference Vegetation Index (NDVI) improves classification accuracy. Namin et al. [20] proposed an automatic system for material classification in natural environments by using multi-spectral images consisting of six visual and one NIR band. The combination of RGB and hyperspectral data, using the same hyperspectral snapshot cameras we use, was evaluated by Cavigelli et al. [8] on data with static background and a very small dataset utilizing deep neural nets.

### 3 Sensor Setup

In this work we used the MQ022HG-IM-SM4X4-VIS (VIS) manufactured by Ximea with an image chip from IMEC [12] utilizing a snapshot mosaic filter which has a per-pixel design. The filters are arranged in a rectangular mosaic pattern of  $n$  rows and  $m$  columns, which is repeated  $w$  times over the width and  $h$  times over the height of the sensor. These sensors are designed to work in a specific spectral range which is called



(a) Example raw image taken by the VIS camera.



(b) A schematic representation of a hypercube and an interpolated plot of a single data point.

**Fig. 1.** Raw image VIS camera with visible mosaic pattern. And a schematic representation of a hypercube.

the active range which is 470–620 nm for the current sensor. The VIS camera has a mosaic pattern with  $n_{\text{VIS}} = 4, m_{\text{VIS}} = 4$ . Ideally every filter has peaks centered around a defined wavelength spectrum with no response outside. However contamination is introduced into the response curve and the signal due to physical constraints. These effects can be summarized as a spectral shift, spectral leaking, and crosstalk and need to be compensated.

Therefore the raw data captured by the camera needs a special preprocessing. We need to construct a hypercube with spectral reflectances from the raw data. This step consists of cropping the raw-image to the valid sensor area, removing the vignette and converting to a three dimensional image, which we call a *hypercube*. Reflectance calculation is the process of extracting the reflectance signal from the captured data of an object. The purpose is to remove the influence of the sensor characteristics like quantum efficiency and the illumination source on the hyperspectral representation of objects. We define a hypercube as  $\mathcal{H}: \mathcal{L}_x \times \mathcal{L}_y \times \mathcal{L}_\lambda \rightarrow \mathbb{R}$  where  $\mathcal{L}_x, \mathcal{L}_y$  are the spatial domain and  $\mathcal{L}_\lambda$  the spectral domain of the image. A visual interpretation of such a hypercube is displayed in Fig. 1b. The hypercube is understood as a volume, where each point  $\mathcal{H}(x, y, \lambda)$  corresponds to a spectral reflectance. Derived from the above definition a spectrum  $\chi$  at  $(x, y)$  is defined as  $\mathcal{H}(x, y) = \chi$ , where  $\chi \in \mathbb{R}^{|\mathcal{L}_\lambda|}$  and  $|\mathcal{L}_\lambda| = n \cdot m$ . The image with only one wavelength, called a spectral band  $\mathcal{H}(z) = \mathcal{B}_{\lambda=z}$ , is defined as follows:  $\mathcal{B}_\lambda: \mathcal{L}_x \times \mathcal{L}_y \rightarrow \mathbb{R}$ . This image contains  $\mathbf{x} = (x, y)$  the wavelength sensitivity  $\lambda$  for each coordinate.

## 4 Classification Framework

For the evaluation of the different features, the image data is first segmented using the SLIC-Superpixels algorithm [1]. This technique joins pixels to a segment based on distance in color and image space. As it is proposed for RGB images, conversion to CIE-LAB color space is recommended to model human perception when measuring color similarity. As aesthetic properties aren't relevant for classification, the euclidean distance of the spectral vectors is used as the measure of similarity. Segmentation ensures homogeneous classification results and redundantizes post-processing. A representative

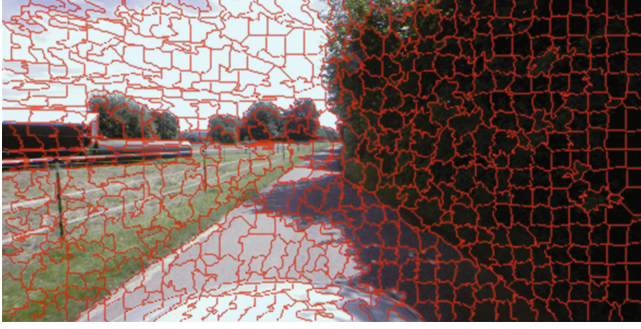


**Fig. 2.** RGB simulation of a hyperspectral image overlaid with the segmentation mask. The edge length is set to 15 pixels, resulting in segments covering approximately 225 pixels each.

segmentation result is shown in Fig. 2. The classifier used for evaluation is the Random Forest algorithm [3]. The image data was recorded using the *VIS* camera mounted on a car combined with several other sensors. For training and verification purposes the images need to be accordingly annotated. The other sensor's recorded data is supposed to be fused with the classification results in further works.

## 5 Extraction of Hyperspectral Features

Our main purpose in this work is the classification of hyperspectral data with  $k$  bands, utilizing spatial and spectral dimensions. To obtain good results and improve classification, features need to be extracted, which contain additional information to the raw spectra in the hypercube. A major source of error is the variable illumination of the scene, because our sensor measures reflectance values which change with illumination changes. So in practice classifiers are trained and may be used on data that shows different illumination situations. By using the normalized spectrum as a feature, we reduce the influence of scene illumination and other irregularities by making use of the hyperspectral counterpart to the log-chromaticity representation of RGB images [11]. In the RGB case, normalization of the values of pixel  $\chi$  by the geometric mean

$$\chi^M(x, y) = \sqrt[3]{\prod_{i=1}^3 \mathcal{B}_i(x, y)} \quad (1)$$

of its components at position  $(x, y)$  is recommended. In the hyperspectral case, the number of bands is much higher, which can cause numerical instabilities, computation of the high-order roots being the cause. Instead the normalization by the sum of the spectrum's  $n$  values

$$\chi^S(x, y) = \sum_{i=1}^n \mathcal{B}_i(x, y) \quad (2)$$

can be used [13]. Logarithmizing isn't necessary for the feature extraction, as the particular axis in the resulting feature space wouldn't gain in variance. Hence the normalized spectrum at image position  $(x, y)$  is computed as

$$\mathcal{B}'_k(x, y) = \frac{\mathcal{B}_k(x, y)}{\chi^S(x, y)} \quad (3)$$

for each spectral band  $k$ . Additionally, the sum of all the spectrum's components  $\chi^S$  is added to the feature vector to represent it's brightness.

To extend the feature space using the textures present in the images, a gabor filter bank is used. Each filter kernel is generated by modulating a gaussian by a sine and cosine term [19]. That way a set of uniformly spread kernels in orientation, scale and frequency are generated. Scale and frequency are inversely proportional. The higher the frequency of the kernel, the lower the scale, the bandwidth of the gaussian is chosen. This ensures the best possible trade-off between localization in frequency space and image space. For the available images, 6 orientations for the kernels with 6 combinations of scale and frequency each were used. The resulting filter bank can be seen in Fig. 3. In natural environments textures representing the same material are often oriented differently, for example blades of grass may be sloped to the side instead of standing straight. For that reason, the coefficients of the same frequency and scale but different directions are combined. Only the maximum coefficient of the multiple orientations for each frequency and kernel scale will be added to the feature vector. With 6 scales used for each orientation, 6 features per spectral band would amount to the feature vector. With the large number of available spectral components in hyperspectral images, it may still exhibit excessively high dimensionality. The dataset used for training and classification, which mainly shows dirt and tarmacked roads in rural areas, holds little difference in texture between the various channels. For that reason, a set of grayscale gabor-features is computed instead of applying the filter bank to each band individually. The underlying grayscale image representation is composed of the mean of the spectral components for each image position.

To obtain a more abstract texture feature, the ripple and granularity are taken into account. Based on the same filter bank and the same grayscale input image, for each combination of frequency and scale the maximum coefficient of the available orientations is extracted. Then the standard deviation between that maximum and the mean coefficient of the available orientations is computed and added to the feature vector. Surfaces with considerable ripple will result in a high value for the respective frequency. Low values occur when the pictured surface exhibits smooth or coarsely granular texture, so it shows no distinguishable orientation. In combination with the grayscale gabor features a wide range of possible texture situations can be represented in the feature space.

Additionally domain knowledge can be used to improve classification accuracy. The image situation for a driving vehicle shows constant conditions, for example sky is typically in the upper part of the image, while navigable terrain will not be found there. Including gravity-based information can support classification by modeling these conditions [15]. The probabilities of all possible class affiliations for each y-coordinate are extracted from the available ground truth images and stored in a lookup table. For feature

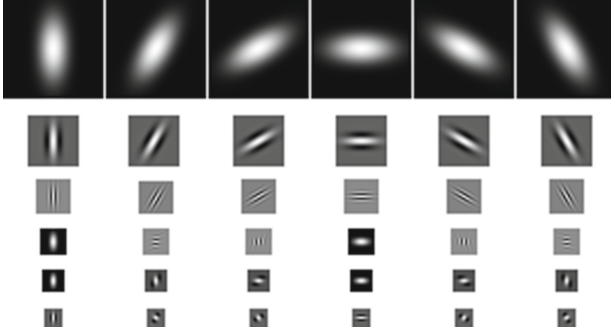


**Fig. 3.** Filter kernels computed for the gabor texture features.

extraction, the probabilities for individual class affiliations for the image position's y-coordinate is read off the lookup table and stored in the feature vector. This feature is restricted to the particular scenario described. Other navigation situations, like flight control of a drone, exhibit different vertical arrangements of scene components. Nevertheless it was used to show how it affects the other features' classification accuracy when paired with them. The proposed features are extracted from a segmented image as described in Sect. 4. The samples for the gabor based texture features and the gravity-based ones are picked from the center of the particular segment. The center  $p^c$  is defined using the 1st order moment as in

$$p^c = \frac{1}{n} \sum_{i=0}^n p_i \quad (4)$$

for the  $n$  2-dimensional coordinates  $p$  in image space that make up the segment. It can also be understood as the center of mass. For the normalized spectrum, the segment's sample isn't extracted from the center, but computed for each pixel and then the mean value for each band is returned. So we obtain a 32-dimensional feature vector for every segment if all features are used, the normalized spectra consisting of the 15 normalized bands and the sum of all bands. Both gabor features contribute six variables, as six scales and frequencies are available in the filter bank. The gravity-based feature offers a variable for each class to be recognized, totaling in 4 variables in our case.

## 6 Evaluation

As far as we know, there is no publicly available data set with hyperspectral data recorded by the MQ022HG-IM-SM4X4-VIS camera, which uses snapshot mosaic technique to acquire hyperspectral data. So we had to build a new dataset on our own, which will be published in the near future. We equipped a standard car with the camera manufactured by Ximea and collected a total of  $\approx 200$  GB of data driving through suburban and rural areas, from which we selected a subset for labeling hyperspectral data. The dataset was labeled in terms of drivability as illustrated in Fig. 4b. The main classes are drivable, rough and obstacle. In addition a sky class was introduced, because it is an



important part of our scene and defines the border of the terrain. It consists of more than 1750000 sky, 1890000 drivable, 1070000 rough and 2910000 obstacle samples. During the labeling process not all image pixels have been assigned classes. This is due to the fact that border areas between materials are not unambiguously assignable. The feature extraction is realized as previously described in Sect. 5. The classifier used for evaluation is the Random Forest algorithm [3], which has proven to be successful in previous experiments [24]. For training, every fifth image in the available set was labeled and used to extract features. This way the training data represents the different possible image situations. The rest of the images was classified using all the different feature vectors. The overall accuracy is computed as  $h/p$ , with  $h$  being the sum of all correctly classified pixels in all images and  $p$  being the total population, made up of all labeled image pixels. Pixels that lack a label are classified as well, but for quantitative evaluation they need to be discarded. When merely using mean spectra of the segments as features, classification fails in some places due to different sources of error. In Fig. 4c the misinterpretation of shadows as obstacles and the sky's reflection on the engine hood as actual sky can be seen. The classification using the normalized mean spectra performs much better in the particular image showed in Fig. 4d. Shaded areas are recognized correctly in most cases and other details match the ground truth better as well. The overall accuracy of this classifier was 91.38%, while the one using the plain mean spectra of the segments achieved 88.92% mean accuracy for the available images. A lot of these images contain less challenging lighting situations, which explain the smaller difference in overall accuracy compared to the one displayed in Fig. 4.

#### **Feature vectors as proposed in this work:**

- A Plain spectra
- B Normalized spectra
- C Grayscale gabor
- D Ripple and granularity
- E Normalized spectra and gravity-based feature
- F All proposed features

#### **Feature vectors as proposed by Namin et al. [20]:**

- G GLCM
- H GLCM and plain spectra
- I Plain spectra, std. deviation in segment, GLCM and fourier features

The other proposed features perform rather poor if they are used exclusively. The gravity-based feature can in no way represent the scene's content, while the grayscale gabor feature reaches an overall accuracy of 79.52%. The ripple and granularity feature performs similarly with 80.46% accuracy. Because the plain coefficients spring from image data that hasn't been normalized, they also depend on actual brightness. That causes the classification to misinterpret shaded areas just like the plain mean spectra. In combination with the normalized spectrum, better classification results can be achieved. The texture features offered only minor improvements, while the combination of normalized spectra and the gravity-based feature exceeded the other possible combinations at 94.82% accuracy. However, the classification results also show errors, that originate



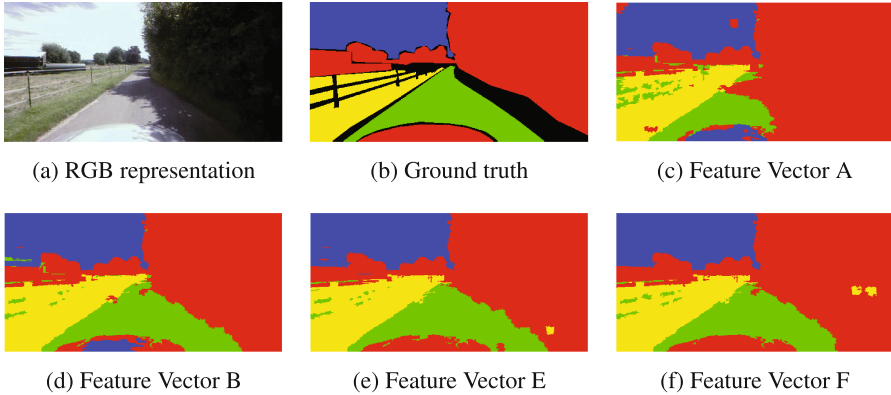


**Fig. 4.** Comparison of classification using plain mean spectra, normalized mean spectra, and combinations of features. For the plain mean spectra the accuracy for the shown image was 85.3%. Normalized mean spectra improved the accuracy to 95.8% in this case. The combination of normalized mean spectra and gravity-based feature offers 97.78%, the combination of all features 97.28% for the shown image. Annotations for navigability analysis are as follows: Green represents good and yellow fair navigability. Red shows obstacles and blue areas picture the sky. (Color figure online)

from the use of this feature. In particular, a lot of segments that are on similar height with the engine hood are classified as obstacles. The reason for this is that in training data the aforementioned engine hood is annotated as obstacle as well. The classification results in Fig. 5 all show that artifact on the right side of the engine hood. Generally, the gravity-based feature might translate poorly to other image situations.

For comparison, some of the features described in [20] were implemented and used for classification in the same fashion. The overall accuracy of 83.48% is worse than the one achieved with simple mean spectra. There are multiple reasons: Shadows weren't treated like in the original paper by annotating them in training. The results shown in Fig. 5 confirm that, as most shadowed areas are classified as obstacles. Furthermore, the feature used for vegetation recognition [2] isn't available because the *VIS* camera used in this work doesn't detect infrared light. These two approaches were essential for the great results that were attained. Also 15 instead of 7 bands in total were available and computing the GLCM for all of them might not add relevant information. Finally the features described in [20] are computed on neighborhood blocks for each pixel. As we used segmentation and created only one feature vector for each segment, for comparison, in this work the kernel sizes of the fourier features and the neighborhood to consider in GLCM were limited to the size of the segment. The scale of these was smaller than the block size proposed by Namin et al. [20], just as the input images are smaller than theirs. Especially the fourier features might yield better results on higher resolution images (Tables 1, 2 and 3).

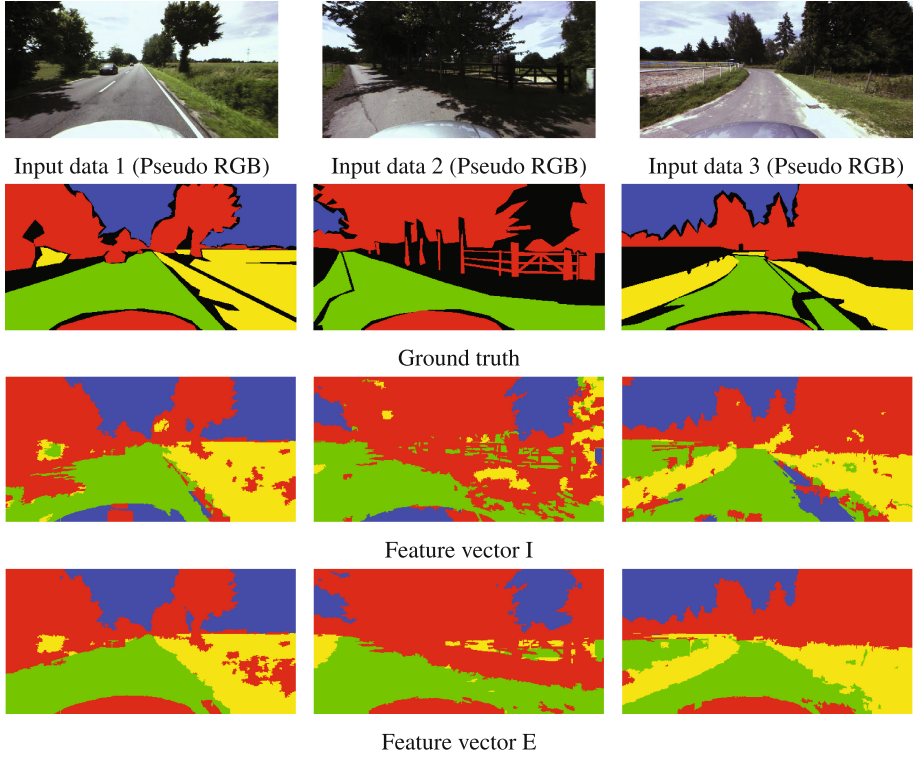


**Fig. 5.** Comparison of classification results. The columns show an RGB representation of the hyperspectral input image, the ground truth, the feature vector proposed by [20] and the combination of normalized spectra and the gravity-based feature presented in this work.

**Table 1.** Comparison of accuracies achieved in classification using different feature vectors.

Feature set	A	B	C	D	E	F	G	H	I
Accuracy	88.92%	91.38%	79.52%	80.46%	94.82%	94.68%	81.15%	83.17%	83.48%

**Table 2.** Precision

Class	Feature vectors								
	A	B	C	D	E	F	G	H	I
Sky	82.02%	83.95%	75.24%	75.11%	89.17%	89.65%	80.45%	81.42%	81.94%
Drivable	81.18%	84.48%	69.53%	69.58%	86.09%	85.76%	67.39%	75.08%	74.70%
Rough	66.41%	66.31%	49.67%	52.34%	66.68%	64.48%	59.34%	54.78%	56.11%
Obstacle	67.97%	70.26%	65.39%	66.38%	74.01%	74.56%	63.44%	64.58%	64.52%

**Table 3.** Recall

Class	Feature vectors								
	A	B	C	D	E	F	G	H	I
Sky	97.22%	97.67%	94.18%	92.63%	98.26%	98.15%	88.42%	94.55%	94.22%
Drivable	89.63%	93.88%	70.65%	74.12%	97.10%	97.20%	84.21%	78.79%	78.58%
Rough	76.16%	79.72%	65.39%	67.02%	83.75%	83.64%	64.99%	73.76%	73.37%
Obstacle	88.03%	90.12%	81.39%	82.12%	95.41%	95.09%	80.36%	81.93%	83.23%

## 7 Conclusion

Both spectral and spatial information have been investigated for classification of hyperspectral images captured with snapshot mosaic cameras. The proposed features are easy to extract, which allows their use in real-time terrain classification. Based on the captured hyperspectral data we were able to precisely distinguish road or drivable areas from non-drivable areas like rough terrain or obstacles. This could greatly enhance terrain classification performance. Especially the use of the normalized mean spectra improved the overall accuracy in a way that would enable actual navigation. Although the proposed gabor texture features didn't improve the accuracy enough to justify their use, the extraction of ripple and granularity turned out to be an efficient way to reduce the dimensionality in feature space while retaining relevant information for classification. In other scenarios and situations, or used on the normalized data as well, the texture features might be more powerful. The adaption of a segmentation algorithm that has been widely used on RGB images for hyperspectral data has been shown and yielded satisfying results.

Further work might validate the benefit of classification on segmented images, especially when the results need to be fused with data from other sensors. For better comparability with other approaches that extract features from hyperspectral data, both the features proposed here and the ones from referenced work need to be validated on a data set that is fully compatible.

## References

1. Achanta, R., Shaji, A., Smith, K., Lucchi, A., Fua, P., Süsstrunk, S.: Slic superpixels compared to state-of-the-art superpixel methods. *IEEE Trans. Pattern Anal. Mach. Intell.* **34**(11), 2274–2282 (2012)
2. Bradley, D.M., Unnikrishnan, R., Bagnell, J.: Vegetation detection for driving in complex environments. In: 2007 IEEE International Conference on Robotics and Automation, pp. 503–508. IEEE (2007)
3. Breiman, L.: Random forests. *Mach. Learn.* **45**(1), 5–32 (2001)
4. Brown, M., Süsstrunk, S.: Multi-spectral sift for scene category recognition. In: IEEE Conference on Computer Vision and Pattern Recognition (CVPR), pp. 177–184. IEEE (2011)
5. Camps-Valls, G., Bruzzone, L.: Kernel-based methods for hyperspectral image classification. *IEEE Trans. Geosci. Remote Sens.* **43**(6), 1351–1362 (2005)

6. Camps-Valls, G., Gomez-Chova, L., Muñoz-Marí, J., Vila-Francés, J., Calpe-Maravilla, J.: Composite kernels for hyperspectral image classification. *IEEE Geosci. Remote Sens. Lett.* **3**(1), 93–97 (2006)
7. Camps-Valls, G., Tuia, D., Gómez-Chova, L., Jiménez, S., Malo, J.: Remote sensing image processing. *Synth. Lect. Image Video Multimedia Process.* **5**(1), 1–192 (2011)
8. Cavigelli, L., Bernath, D., Magno, M., Benini, L.: Computationally efficient target classification in multispectral image data with deep neural networks. In: *SPIE Security+Defence*. p. 99970L. International Society for Optics and Photonics (2016)
9. Chetan, J., Krishna, M., Jawahar, C.: Fast and spatially-smooth terrain classification using monocular camera. In: *Pattern Recognition (ICPR)*, 2010 20th International Conference on. pp. 4060–4063. IEEE (2010)
10. Fauvel, M., Benediktsson, J.A., Chanussot, J., Sveinsson, J.R.: Spectral and spatial classification of hyperspectral data using SVMs and morphological profiles. *IEEE Trans. Geosci. Remote Sens.* **46**(11), 3804–3814 (2008)
11. Finlayson, G.D., Hordley, S.D., Lu, C., Drew, M.S.: On the removal of shadows from images. *IEEE Trans. Pattern Anal. Mach. Intell.* **28**(1), 59–68 (2006)
12. Geelen, B., Tack, N., Lambrechts, A.: A compact snapshot multispectral imager with a monolithically integrated per-pixel filter mosaic. In: *SPIE Moems-Mems*. p. 89740L. International Society for Optics and Photonics (2014)
13. Gevers, T., Stokman, H., Weijer, J.v.d.: Colour constancy from hyper-spectral data. In: *Proceedings of the British Machine Vision Conference*, pp. 30.1–30.10. BMVA Press (2000)
14. Hughes, G.: On the mean accuracy of statistical pattern recognizers. *IEEE Trans. Inf. Theory* **14**(1), 55–63 (1968)
15. Javanbakhti, S., Zinger, S., de With, P.H.N.: Context-based region labeling for event detection in surveillance video. In: *2014 International Conference on Information Science, Electronics and Electrical Engineering*, vol. 1, pp. 94–98, April 2014
16. Li, J., Bioucas-Dias, J.M., Plaza, A.: Semisupervised hyperspectral image segmentation using multinomial logistic regression with active learning. *IEEE Trans. Geosci. Remote Sens.* **48**(11), 4085–4098 (2010)
17. Li, J., Bioucas-Dias, J.M., Plaza, A.: Spectral-spatial hyperspectral image segmentation using subspace multinomial logistic regression and markov random fields. *IEEE Trans. Geosci. Remote Sens.* **50**(3), 809–823 (2012)
18. Melgani, F., Bruzzone, L.: Classification of hyperspectral remote sensing images with support vector machines. *IEEE Trans. Geosci. Remote Sens.* **42**(8), 1778–1790 (2004)
19. Naghdy, G.A., Wang, J., Ogunbona, P.O.: Texture analysis using gabor wavelets, vol. 2657, pp. 74–85 (1996)
20. Namin, S.T., Petersson, L.: Classification of materials in natural scenes using multi-spectral images. In: *2012 IEEE/RSJ International Conference on Intelligent Robots and Systems (IROS)*, pp. 1393–1398. IEEE (2012)
21. Plaza, A., Benediktsson, J.A., Boardman, J.W., Brazile, J., Bruzzone, L., Camps-Valls, G., Chanussot, J., Fauvel, M., Gamba, P., Gualtieri, A., et al.: Recent advances in techniques for hyperspectral image processing. *Remote Sens. Environ.* **113**, S110–S122 (2009)
22. Salamati, N., Larlus, D., Csürka, G.: Combining visible and near-infrared cues for image categorisation. In: *Proceeding of the 22nd British Machine Vision Conference (BMVC 2011)*, No. EPFL-CONF-169247 (2011)
23. Tarabalka, Y., Fauvel, M., Chanussot, J., Benediktsson, J.A.: SVM-and MRF-based method for accurate classification of hyperspectral images. *IEEE Geosci. Remote Sens. Lett.* **7**(4), 736–740 (2010)
24. Winkens, C., Sattler, F., Paulus, D.: Hyperspectral terrain classification for ground vehicles. In: *12th International Conference on Computer Vision Theory and Applications (VISAPP)* (2017)

Computer Analysis of Images and Patterns  
17th International Conference, CAIP 2017, Ystad,  
Sweden, August 22-24, 2017, Proceedings, Part I  
Felsberg, M.; Heyden, A.; Krüger, N. (Eds.)  
2017, XVI, 413 p. 156 illus., Softcover  
ISBN: 978-3-319-64688-6